The 2nd International Symposium on Urban Lifeline Saitama, Japan 7.18~20, 2025.

Seismic energy distribution and fragility assessment of reinforced concrete multi-span highway bridges

Muhammad Rashid[1], Mayuko Nishio[2]

[1] Ph.D. Student, Department of Engineering Mechanics and Energy, University of Tsukuba, Tsukuba, Japan.
[2] Associate Professor, Institute of Systems and Information Engineering, University of Tsukuba, Tsukuba, Japan.

ABSTRACT

The seismic resilience of highway bridges is critical to ensuring the safety and functionality of transportation networks during earthquakes. The quantification and distribution of seismic energy associated with seismic hazards is imperative for structural performance evaluation and is crucial for understanding the structural behavior until collapse. This study aims to investigate the seismic energy dissipation patterns, including hysteretic and damping energy, at the component and global structural level and assess the fragility of a reinforced concrete (RC) multi-span highway bridge. For this purpose, a high-fidelity finite element model was developed, and an extensive non-linear time history analysis was carried out for the given ground motion suite. The energy dissipation mechanisms are quantified for key bridge components, such as columns, bearings, deck unseating, and shear keys. The relative contribution of each component to global hysteretic and damping energy dissipation is investigated. Fragility curves, which establish the likelihood of different damage states for the given seismic hazard, are developed using probabilistic seismic demand models for the bridge components and system. Results reveal that hysteretic energy dissipation dominates the response of RC bridges, particularly in bearings. Damping energy exhibits a more stable response and is dominated by the structural mass and bearing. The fragility analysis indicates that the component with high energy dissipation is the governing component. Similarly, components with the least energy dissipation show reduced probabilities of exceeding critical damage thresholds. The proposed energy-based fragility framework enhances understanding of seismic demand distribution in RC bridge systems and offers valuable insights for the development of performance-based design and retrofitting strategies, contributing to the broader goal of resilient infrastructure in seismic-prone regions.

Keywords: seismic energy, hysteretic, damping, fragility, highway bridges

1. INTRODUCTION

Reinforced concrete multi-span highway bridges are vital components of transportation networks, playing a central role in sustaining regional socio-economic activities and ensuring functionality during emergency response. However, their vulnerability to seismic events continues to be a critical concern, largely due to the complex dynamic interactions among structural components and the inherent uncertainties associated with earthquake ground motions. Major seismic events such as the 1994 Northridge (USA), 1995 Kobe, 2011 Tohoku (Japan), and 2023 Turkey-Syria earthquakes have repeatedly exposed the fragility of bridge infrastructure, underscoring the urgent need for more robust seismic risk assessments and resilient design methodologies [1]. Mitigating earthquake-induced damage requires a comprehensive understanding of seismic hazards and their interaction with structural systems. While conventional force- and displacement-based design approaches evaluate structural performance in terms of peak force and deformation, they often fail to capture the cumulative and energy-dependent nature of seismic demands. In contrast, energy-based seismic design offers a more holistic solution by simultaneously accounting for force, deformation, and energy input, thus providing a more realistic representation of structural behavior under seismic excitation [2].

The distribution and dissipation of seismic energy are central to understanding damage mechanisms in bridge components such as piers, bearings, shear keys, and deck connections. These energy pathways dictate how damage initiates and propagates across the structure. Kinetic and damping energies, which correspond to the structure's velocity-dependent response, together with hysteretic energy, arising from inelastic deformation, provide critical insight into how individual components contribute to the overall energy dissipation during seismic loading [3]. Importantly, energy-based demand parameters can differentiate between same components subjected to similar displacements but experiencing distinct internal forces, enabling more accurate assessment of serviceability and damage potential.

Unlike peak-based engineering demand parameters (EDPs), which may overlook the cumulative effects of ground motion, energy-based EDPs offer a means of capturing the full seismic demand history. Although cumulative EDPs have been adopted in various studies to enhance fragility modeling [4–6], defining consistent damage state thresholds remains a challenge. Displacement-based EDPs, by contrast, often allow clearer threshold definition, however, may miss critical energy-related damage phenomena. Bridging this gap, studies such as Quinde et al. [7] and Gentile et al. [3] have explored correlations between deformation- and energy-based metrics in frame systems. Their findings suggest that energy-based models, when linked to seismic intensity measures, can provide state-dependent fragility estimates. However, these approaches are typically limited to single-degree-of-freedom or frame systems and do not fully capture the distributed demands in complex bridge structures.

In this context, fragility analysis serves as a probabilistic tool to quantify the likelihood of structural systems exceeding specific damage states under varying seismic intensities. Despite their utility, conventional fragility approaches often neglect the influence of seismic energy demand and dissipation, thereby reducing the robustness and reliability of vulnerability estimates. To address this limitation, the present study investigates the distribution and dissipation of seismic energy in RC multi-span highway bridges, with the objective of extending classical fragility frameworks to incorporate energy-based demand parameters explicitly. The findings offer improved insights into energy-driven damage processes and significantly contribute to refining existing seismic fragility models for critical transportation infrastructure.

2. SEIMIC ENERGY DISTRIBUTION IN STRUCTURE

The balance between earthquake input energy and the energy absorbed by a structure offers a straightforward way to assess structural behavior up to failure. Earthquake input energy (*IE*), which reflects the intensity of ground motion, is distributed within the structure as kinetic energy (*KE*), damping energy (*DE*), strain energy (*SE*), and hysteretic energy (*HE*). This energy balance can be represented by Eq. (1).

$$IE = KE + DE + SE + HE \tag{1}$$

Various methods exist to compute energy components; however, this study employs the direct integration method. For multi-degree-of-freedom (MDOF) systems with $[\mathbf{m}]$ and $\dot{\mathbf{u}}$ as the mass matrix and velocity vector respectively, the corresponding formulations are presented herein. Kinetic energy, representing the work done by inertial forces, is defined in Eq. (2).

$$KE = \frac{1}{2}\dot{\mathbf{u}}^{\mathrm{T}}[\mathbf{m}]\dot{\mathbf{u}} \tag{2}$$

A portion of the energy is dissipated through damping forces and can be calculated using the expression for work done by inherent structural damping. If $[\mathbf{c}]$ is the damping matrix of the system, then the damping energy is given by Eq. (3)

$$DE = \int_0^u \mathbf{d}\dot{\mathbf{u}}^{\mathrm{T}}[\mathbf{c}]\dot{\mathbf{u}} = \int_0^t \dot{\mathbf{u}}^{\mathrm{T}}[\mathbf{c}]\dot{\mathbf{u}}dt \tag{3}$$

The energy absorbed by the system consists of elastic strain energy and hysteretic energy. Strain energy is associated with the elastic response during loading and is influenced by stiffness, strength, and deformation. In contrast, hysteretic energy reflects the energy dissipated through inelastic behavior during cyclic loading. Both *SE* and *HE* can be estimated based on the component's overall deformation response. Strain energy can be computed at any point during loading by tracking stiffness variations along the force-deformation curve, as expressed in Eq. (4).

$$SE = \frac{1}{2}\mathbf{u}^{T}[\mathbf{k}_{\mathbf{t}}]\mathbf{u} \tag{4}$$

where $[\mathbf{k}_{\mathbf{t}}]$ is the tangent stiffness matrix and $\mathbf{u}$ is the displacement vector of the system.

Hysteretic energy can be obtained as the difference between the total absorbed energy and the strain energy, when the system is under external force $\mathbf{F}$, as in Eq. (5).

$$HE = \int_0^u \mathbf{F}^{\mathbf{T}} \mathbf{du} - \frac{1}{2}\mathbf{u}^T \left[\mathbf{k_t}\right]\mathbf{u} \tag{5}$$

Seismic input energy is governed by structural mass and ground motion acceleration. When mass is concentrated at the nodes and element mass is neglected, *IE* can be calculated based on the interaction between ground acceleration and nodal mass, assuming a uniform excitation. However, this approach ignores phase delays, which can significantly affect the accuracy of results in large structures. For the ground motion acceleration $\ddot{\mathbf{u}}_\mathbf{g}$,the *IE* is given as follows.

$$IE = -\int_0^u \mathbf{du}^{\mathbf{T}} \left[\mathbf{m}\right]\ddot{\mathbf{u}}_\mathbf{g} = -\int_0^t \dot{\mathbf{u}}^{\mathbf{T}} \left[\mathbf{m}\right]\ddot{\mathbf{u}}_\mathbf{g} dt \tag{6}$$

3. FRAGILITY ANALYSIS

Fragility functions apply reliability theory to evaluate the seismic risk of civil infrastructure by quantifying the probability that seismic demand (*D*) exceeds structural capacity (*C*) for a given ground motion intensity (*IM*) [8]. This relationship can be expressed mathematically as follows.

$$Fragility = P\left[D \geq C \mid IM\right] \tag{7}$$

Seismic demand and structural capacity are typically represented by a PSDM and predefined limit states, respectively. The seismic demand can be estimated using a power-law relationship, as expressed in Eq. (8).

$$S_d = a\left(IM\right)^b \tag{8}$$

where *a* and *b* are regression coefficients, which can be estimated from non-linear time history analysis. Following the lognormal distribution assumption for the capacity limit states the fragility functions of the components can be expressed as in Eq. (9) [9].

$$P\left[D \geq C \mid IM\right] = \Phi\left(\frac{\ln\left(S_d\right) - \ln\left(S_c\right)}{\beta_{d|IM}}\right) \tag{9}$$

where *Sd* and *Sc* are the medians of demand and capacity and $\beta_{d|IM}$ is the dispersion of the components' PSDM.

While component fragility is useful in identifying the most vulnerable components and retrofit decision-making, system fragility is more significant for transportation network risk assessments. Using the first order reliability theory, the bridge system can be regarded as a series or parallel system, depending on the correlation index. If all the components are considered completely correlated, the system failure will be governed by the most fragile component. On the other hand, if no correlation among component responses is considered, the system will be treated as parallel and the system failure under specific limit state will reach once all the components get into that particular limit state. Considering the independent failure assumption of different components $P_i(F)$, the system wide fragility, $Psys(F)$, can be derived using Eq. (10) [8].

$$Psys(F) = 1 - \prod_{i=1}^{m}\left[1 - P_i\left(F\right)\right] \tag{10}$$

4. DESCRIPTION AND NUMERICAL MODELING OF THE BRIDGE

The bridge in this study is representative of the multi-span continuous I-girder RC bridge class, adopted from DesRoches et al. [10]. The typical span length ranges from 9 to 46 m and employs standard I-shaped girders in the superstructure. Specific details and analytical modeling are outlined in the following sections.

4.1. Structural description

A typical seat-type abutment bridge is considered in this study, reflecting common configurations in the California bridge inventory. Given that most I-girder bridges are two- or three-span, a three-span layout is selected, as two-span configurations

have been widely studied [11]. The bridge represents median design values from the 1971–1990 design era. The central span is 18.29 m, which is about 1.4 times longer than the side span. Bent columns are 6.7 m tall, 0.91 m in diameter, and spaced 6.6 m apart. Each column contains 36 #8 longitudinal bars and #4 spiral ties at 89 mm pitch. The superstructure includes seven girders (0.91 m deep, 0.48 m flange width) spaced at 1.68 m intervals. A 25.4 mm gap separates the deck from the abutment backfill, and shear keys are used to limit lateral displacement. Translational and rotational springs having stiffness values of 140.1 x 10^3 kN/m and 3387 x 10^3 kN.m/rad respectively, are provided at the foundation to account for soil structure interaction.

4.2. Numerical modeling

The numerical modeling of the study bridge was conducted using *OpenSees*, incorporating both material and geometric non-linearities [12]. Material properties used in the model are summarized in Table 1. The bridge deck was modeled as an *ElasticBeamColumn* element, with mass concentrated at discrete nodes along its length. Composite section properties were derived from girder geometry and assigned accordingly. A schematic of the analytical model is shown in Fig.1.

Table 1. Material properties of structural components

Bridge component	**Material properties**
Bearings[1]	F_y = 58.5 kN, K = 4.48 kN/mm
Columns	Unconfined concrete: f'_c = 33.8 MPa, ε_c = 0.002, f_t = 3.62 MPa, ε_t = 0.0002
	Confined concrete: f'_c = 42.9 MPa, ε_c = 0.005, f_t = 3.62 MPa, ε_t = 0.0002
	Steel: F_y = 460 MPa, E_s = 2 x10^5 MPa, α = 0.01
Piles[1]	F_y = 124.4 kN, F_u = 177.7 kN, δ_y = 7.6 mm, δ_u = 25.4 mm
Backfill soil[2]	F_u = 444 kN, K = 20.5 kN/mm/m
Shear keys[1]	F_y = 142.2 kN, F_u = 203.1 kN, δ_y = 7.62 mm, δ_u = 25.4 mm
Pounding[1]	K_1 = 2328.7 kN/mm, K_2 = 592.39 kN/mm, Δ_{gap} = 25.4 mm, δ_y = 29.2 mm

[1] The values are associated with a single component.
[2] The mentioned values are per unit width of abutment.

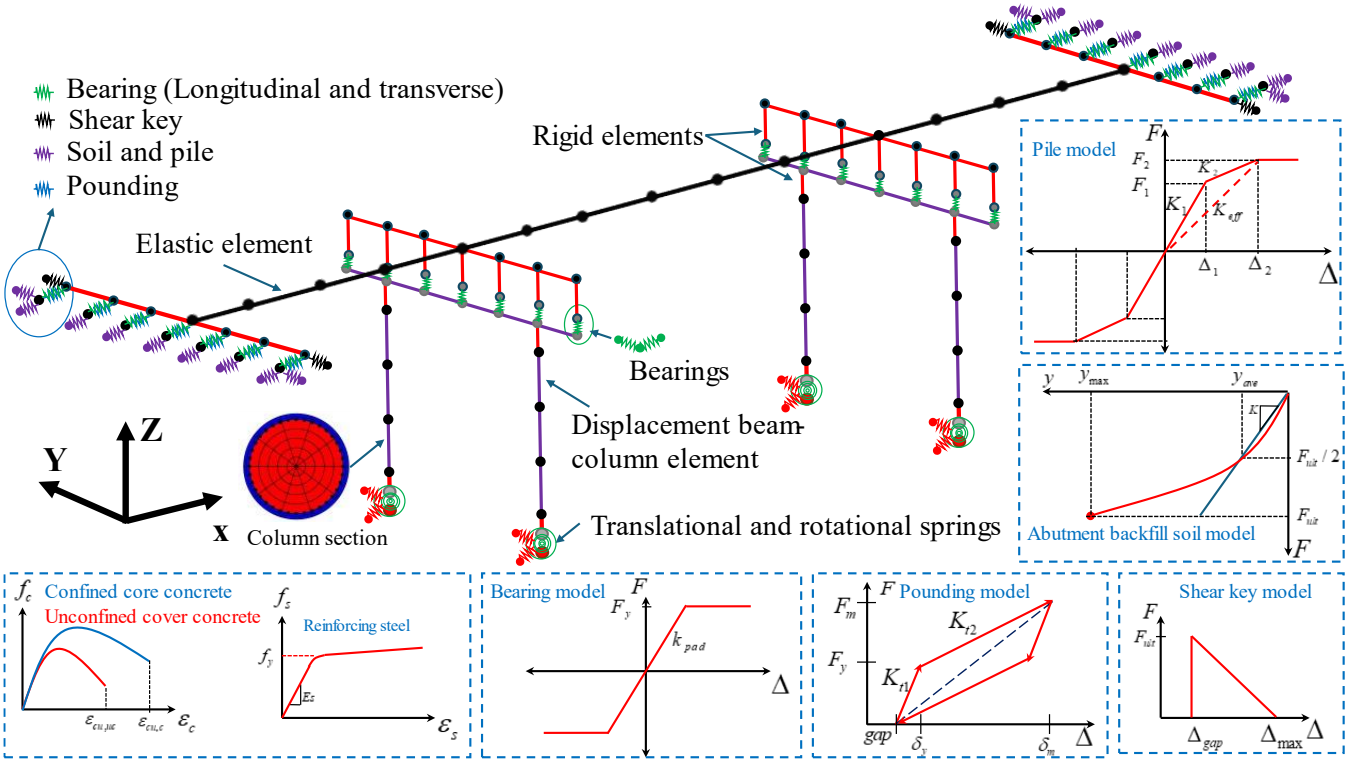

Figure 1. A three-dimensional finite element model of the target bridge

The nonlinear concrete behavior was captured using the *Concrete07* model, based on the Chang and Mander formulation, while *Steel02* was used for reinforcing steel, accounting for isotropic hardening and the Bauschinger effect. Columns were modeled as displacement-based beam-column elements with fiber sections, including P-delta effects. Longitudinal interaction between the bridge deck and abutment leads to concentrated pressure in the backfill soil, which was modeled using

ZeroLengthElements with hyperbolic gap characteristics. Passive resistance from the pile-backfill system was modeled using a tri-linear model, following Choi [13]. Pounding at the deck-abutment interface, which is common in seat-type abutment bridges, was represented by using *ZeroLengthElements* with the *ElasticPPGap* material, oriented normal to the deck face [14], to simulate contact and separation. Isolation bearings were represented as bilinear elastoplastic *ZeroLengthElements*, with a shear modulus of 1.38 MPa and a friction coefficient of 0.4 between the concrete and bearing pad. Shear keys were modeled as *ZeroLengthElements* with hysteretic properties.

5. GROUND MOTION SUITE

To assess the energy characteristics of various bridge components, 269 accelerograms were selected from the K-NET and KiK-net strong ground motion databases. These records span 35 seismic events recorded between 1996 and 2023. The acceleration response spectra of the selected waveforms, along with their median and standard deviation, are presented in Fig. 2 (a). The selection criteria for the dataset included: (1) mean peak ground acceleration (PGA) of the EW and NS components exceeding 0.06 g, (2) moment magnitude ≥ 5.5, (3) focal depth ≤ 70 km, and (4) average shear wave velocity ($Vs30$) between 120 and 1400 m/s. A significant portion of the records originate from the 2011 Tohoku earthquake, contributing to the high spectral accelerations observed in the dataset.

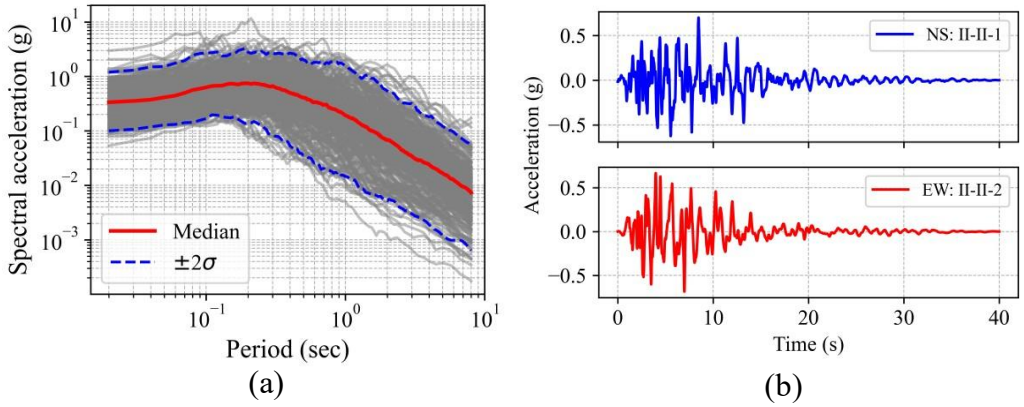

Figure 2. (a) Acceleration response spectra for the selected records (b) Type II-II design record for deterministic analysis

6. RESULTS AND DISCUSSION

6.1. Seismic energy distribution for bridge components

This section discusses the distribution of seismic energy and the contributions of various components to global structural energy. A gravity analysis was first performed, followed by dynamic analysis, with energy computed at each step. For illustration, a deterministic case using the Type II-II design waveform (Fig. 2b) recorded at JR Takatori station during the 1995 Kobe earthquake is considered.

Seismic energy components were calculated following the formulation in Section 2. Damping associated with bearings, columns, deck, piles, and soil was treated as elemental damping, while mass-proportional damping was applied at the nodal level. At the end of excitation, both damping and hysteretic energies plateau, while kinetic energy diminishes to zero. Fig. 3a shows damping energy contributions, where nodal mass damping is the most significant, contributing approximately 1570 kN·m, followed by abutment soil with about 400 kN·m, and bearings with around 195 kN·m. In contrast, the deck and cap beam contribute the least, with about 16 kN·m and 2 kN·m, respectively. Hysteretic energy distribution is shown in Fig. 3b, with bearings contributing the majority (~5560 kN·m) reflecting their role in isolating superstructure inertial forces. Cap beams and columns dissipate less energy due to their higher stiffness. The temporal profile of energy accumulation mirrors the kinetic energy trend (Fig. 3c), with concentration within the first 20 seconds, corresponding to the strong motion phase of the input accelerogram.

At the system level, the sum of damping, hysteretic, and kinetic energies at any time equals the input seismic energy (Fig. 3d). The cumulative hysteretic energy, around 7500 kN·m, is roughly three times greater than the cumulative damping energy, and its growth closely aligns with the high-amplitude segments of the accelerogram. These findings highlight bearings as the most critical energy-dissipating elements, effectively limiting energy transfer to the substructure and playing a key role in structural resilience and post-event maintainability.

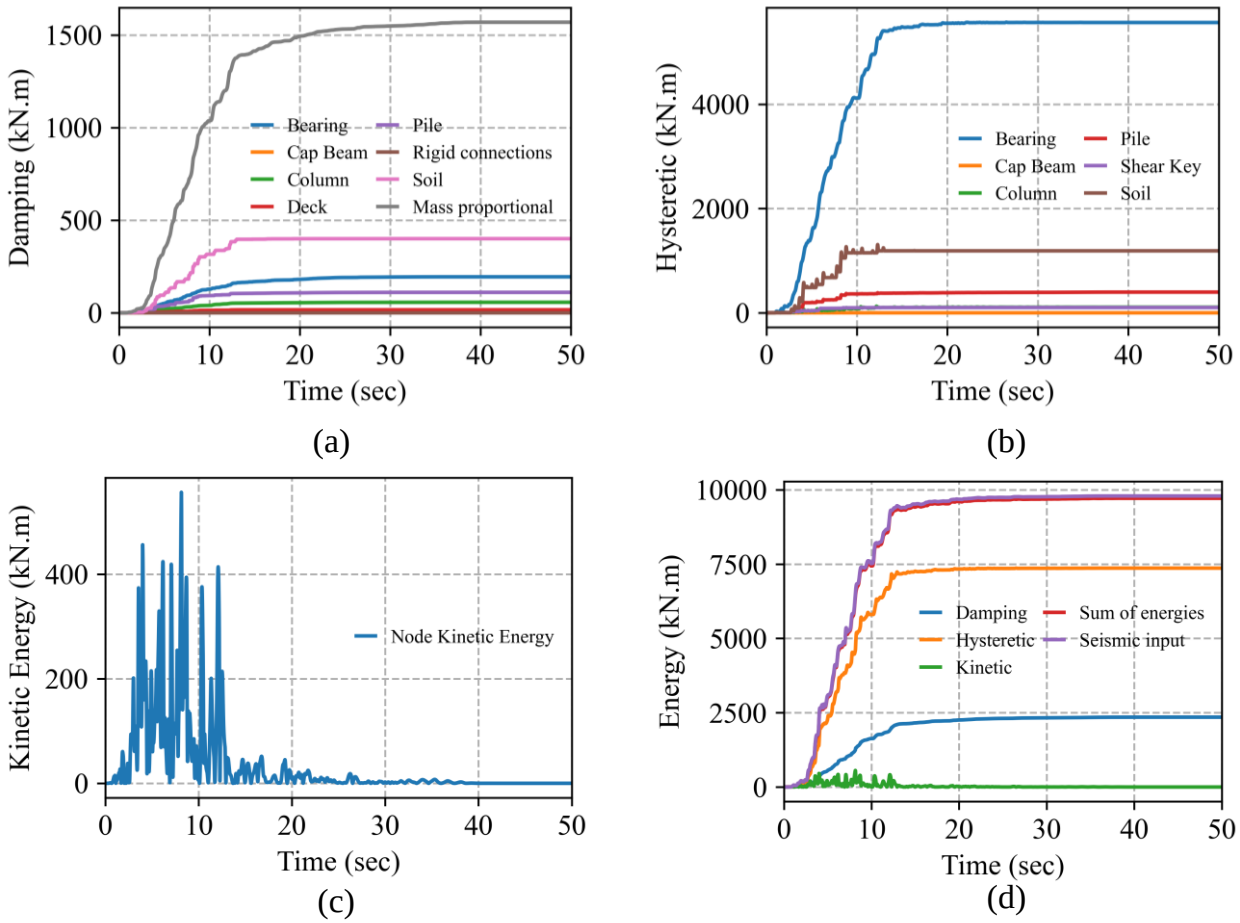

Figure 3. Seismic energy distribution for the bridge model (a) Damping energy (b) Hysteretic energy (c) Kinetic energy and (d) Bridge system energy.

6.2. Bridge components and system's fragility functions

Following extensive nonlinear time-history analyses, the peak responses of critical components were extracted to develop energy-based fragility functions. Initially, energy-based EDPs were defined based on the correlation between the dissipated energy and peak deformation observed for each component, as summarized in Table 2. Following Ramanathan et al. [11], columns and deck unseating were identified as primary components due to their significant influence on the vertical stability of the bridge, and four limit states were defined accordingly. In contrast, bearings and shear keys, which serve as sacrificial elements primarily effective at moderate damage levels, were treated as secondary components.

Fragility functions for all defined limit states across various components are presented in Fig. 4. For the column, the median spectral acceleration values corresponding to slight, moderate, extensive, and collapse limit states are approximately 1.36g, 2.84g, 4.17g, and 5.27g, respectively. In contrast, the median fragility associated with deck unseating reached at lower seismic intensity levels, with values of 0.23g for slight and 1.61g for collapse level. As sacrificial elements, shear keys reach their median fragility at 0.62g for slight damage and 1.68g for collapse. The results further confirm that bearings are the most vulnerable components, owing to their significant role in hysteretic energy dissipation, which further contributes to triggering deck unseating. The relative vulnerability patterns align with the energy distribution trends presented in Fig. 3 emphasize the effectiveness of energy-based EDPs in capturing the cumulative structural response under seismic loading.

Following the component-level fragility assessment, system-level fragility functions were developed for all defined limit states, along with their corresponding distribution parameters, as illustrated in Fig. 6. The system response appears to be strongly influenced by the behavior of the bearings, due to the specific formulation adopted for system-level fragility estimation. The median spectral acceleration values for slight, moderate, extensive, and collapse limit states are approximately 0.13g, 0.53g, 1.27g, and 1.52g, respectively.

Table 2. Equivalent energy-based limit states for bridge components

Component EDP	Slight	Moderate	Extensive	Collapse
Column curvature ductility	1 [24.16]*	2 [79.10]	3.5 [142.09]	5 [224.74]
Deck unseating (mm)	25 [5.22]	75 [98.76]	150 [255.40]	225 [380.09]
Bearing deformation (mm)	25 [2.09]	100 [87.73]	--	--
Shear key deformation (mm)	75 [6.58]	250 [24.26]	--	--

*The values in brackets represent the equivalent dissipated energy (unit: kN·m) corresponding to the given deformation level

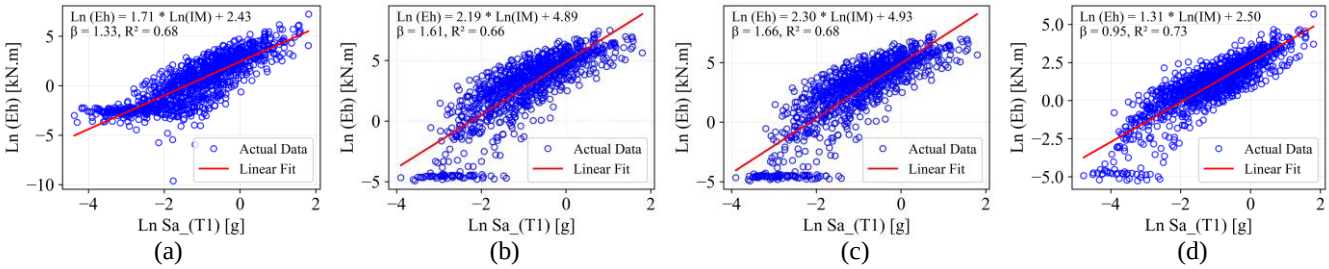

Figure 4. PSDMs for bridge components (a) Column (b) Deck unseating (c) Bearing (d) Shear key

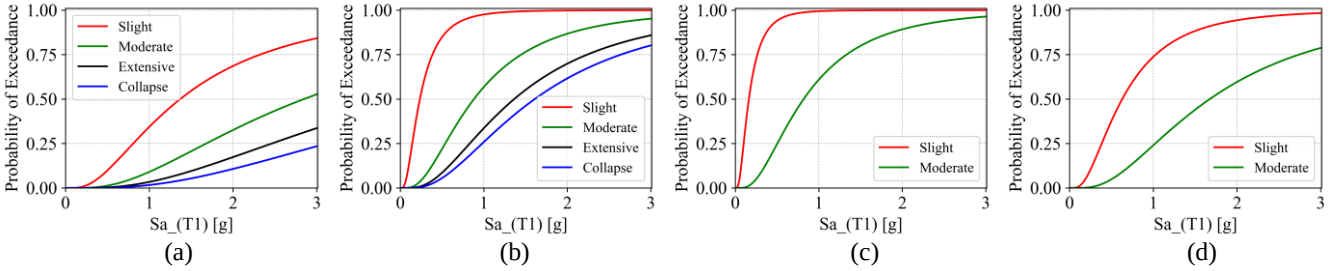

Figure 5. Fragility for bridge components (a) Column (b) Deck unseating (c) Bearing (d) Shear key

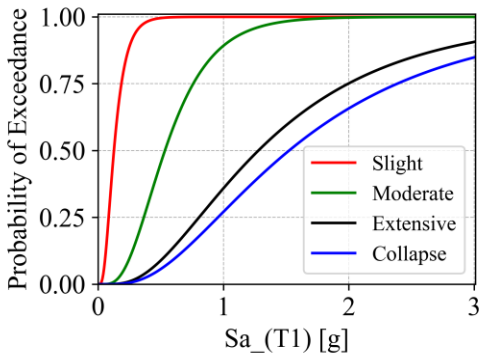

Figure 6. Bridge system fragility curves

7. CONCLUSIONS

This study presents a comprehensive energy-based seismic fragility assessment framework for RC multi-span highway bridges, with an emphasis on understanding energy distribution and component-level contributions to global structural performance. A detailed numerical model was developed , incorporating material and geometric nonlinearities, and was subjected to extensive nonlinear time-history analyses using real recorded ground motions.

Energy-based engineering demand parameters were defined for key bridge components by establishing correlations between cumulative energy dissipation and peak deformation. The study classified components into primary (columns and deck unseating) and secondary (bearings and shear keys) categories, assigning appropriate limit states accordingly. Fragility

functions were developed at both component and system levels. The results indicate that bearings are the most vulnerable components, primarily due to their significant role in hysteretic energy dissipation. Deck unseating was observed to reach at lower seismic intensities compared to column damage, emphasizing the importance of proper isolation and restraint design. System-level fragility was predominantly influenced by bearing response, with median spectral acceleration values of 0.13g, 0.53g, 1.27g, and 1.52g corresponding to slight, moderate, extensive, and collapse limit states, respectively. The proposed energy-based fragility framework effectively captures the cumulative effects of seismic loading and offers a more holistic understanding of bridge performance under strong ground motions. Future research should focus on experimental validation of energy dissipation thresholds for various components and extend the approach to multiple bridge classes to develop a generalized framework. These findings provide valuable guidance for performance-based seismic design, retrofit prioritization, and resilience planning of critical bridge infrastructure in seismically active regions.

REFERENCES

[1] Rashid M, Nishio M. Mainshock–aftershock seismic fragility assessment of civil structures: A state-of-the-art review. Earthquake Engineering and Resilience 2024;3:548–73. https://doi.org/10.1002/eer2.105.

[2] Jamnani HH, Amiri JV, Rajabnejad H. Energy distribution in RC shear wall-frame structures subject to repeated earthquakes. Soil Dynamics and Earthquake Engineering 2018;107. https://doi.org/10.1016/j.soildyn.2018.01.010.

[3] Gentile R, Galasso C. Hysteretic energy-based state-dependent fragility for ground-motion sequences. Earthq Eng Struct Dyn 2021;50. https://doi.org/10.1002/eqe.3387.

[4] Uang C -M, Bertero V V. Evaluation of seismic energy in structures. Earthq Eng Struct Dyn 1990;19. https://doi.org/10.1002/eqe.4290190108.

[5] Kunnath SK, Chai YH. Cumulative damage-based inelastic cyclic demand spectrum. Earthq Eng Struct Dyn 2004;33. https://doi.org/10.1002/eqe.363.

[6] Chai YH. Incorporating low-cycle fatigue model into duration-dependent inelastic design spectra. Earthq Eng Struct Dyn 2005;34. https://doi.org/10.1002/eqe.422.

[7] Quinde P, Terán-Gilmore A, Reinoso E. Cumulative Structural Damage Due to Low Cycle Fatigue: An Energy-Based Approximation. Journal of Earthquake Engineering 2021;25. https://doi.org/10.1080/13632469.2019.1692736.

[8] Nielson BG. Analytical fragility curves for highway bridges in moderate seismic zones. Georgia Tech, 2005. https://doi.org/10.1016/j.engstruct.2017.03.041.

[9] Choi E, DesRoches R, Nielson B. Seismic fragility of typical bridges in moderate seismic zones. Eng Struct 2004;26:187–99. https://doi.org/10.1016/j.engstruct.2003.09.006.

[10] DesRoches R, Padgett J, Ramanathan K, Dukes J. Feasibility Studies for Improving Caltrans' Bridge Fragility Relationships . California: 2012.

[11] Ramanathan K, Padgett JE, DesRoches R. Temporal evolution of seismic fragility curves for concrete box-girder bridges in California. Eng Struct 2015;97:29–46. https://doi.org/10.1016/j.engstruct.2015.03.069.

[12] McKenna F. OpenSees: A framework for earthquake engineering simulation. Comput Sci Eng 2011;13. https://doi.org/10.1109/MCSE.2011.66.

[13] Choi E. Seismic analysis and retrofit of mid-America bridges. 20022002 .

[14] Muthukumar S, DesRoches R. A Hertz contact model with non-linear damping for pounding simulation. Earthq Eng Struct Dyn 2006;35. https://doi.org/10.1002/eqe.557.